RJCE
ISSN:0972-0626

ISSN: 0972-0626
Volume 29, Issue 07, July, 2025

Thermodynamic, Kinetic, Conductivity, and Theoretical DFT Study of Poly (p-Toluidine) and Starch -Grafted Poly (p-toluidine) Copolymer

Khansa Abdul Razzaq Ali Al-Assadi[1]

Department of Chemistry, College of Scince, University of Basrah, Basrah, Iraq[1]

ABSTRACT— Poly (p-toluidine) (PPT) and starch-grafted poly (p-toluidine) copolymer (SGPPT) were synthesized via oxidative polymerization. PPT and SGPPT were prepared using toluidine monomer, starch, hydrochloric acid, ammonium persulfate, and sodium hydroxide. The structure was corroborated through a diverse range of characterization techniques, including field emission scanning electron microscopy (FESEM) and X-ray diffraction (XRD) analysis, which elucidated the crystalline transformation of (PPT) in association with starch-grafted copolymer. The vibrational modes were measured by Fourier-transform infrared spectroscopy (FTIR). UV–Vis Spectrophotometer revealed distinctive peaks indicative of polymer formation and the energy gap from 3.62 eV for un-grafted (PPT) to 2.37 eV for the SGPPT copolymer, as elucidated through the Tauc plot. Thermogravimetric analysis (TGA) was employed to determine thermodynamic and kinetic parameters, demonstrating the first-order reaction kinetics of both polymers. The conductivity of thin films of polymer and copolymer was measured, exhibiting ohmic behavior, with higher conductivity observed in the copolymer. Additionally, a theoretical study for the first time for this polymer and copolymer using density functional theory (DFT) calculations with the B3LYP/6-311++G(d,p) basis set, revealing a relationship between trimers of PPT and SGPPT and the energy gap. Overall, this study demonstrates the successful synthesis and characterization of poly (p-toluidine) and starch-grafted poly (p-toluidine) copolymer, highlighting their potential applications in various fields.

KEYWORDS: Starch-grafted copolymer, Band gap, Electrical conductivity, DFT modeling

DOI:
07.1499/Rjce.30.08.2025.01

1. INTRODUCTION

It is known that the polymers are electrically insulating materials, but they have unique electrical and optical properties similar to inorganic semiconductors, but this feature has changed after scientists reached the possibility of modifying polymers to become good conductors of electricity, similar to metals [1- 3].

Typical conducting polymers include polyacetylene, polyaniline and its derivatives, polyfuran, polypyrrole, polythiophene, and polyphenylene. In general, conductive polymers exhibit low electrical conductivity and limited optical properties in their solid state. It is also possible to change their properties by doping the polymers with appropriate materials. Polyacetylene has a conductivity of about 10^{-5} $\Omega^{-1}.cm^{-1}$, but when the level of doping increases, the conductivity rises to (102-103) $\Omega^{-1}.cm^{-1}$ [4], [5]. Various methods have been used to synthesize the conducting polymers, including electrochemical, chemical oxidative polymerization, vapor phase synthesis, hydrothermal, electrospinning, template-assisted photochemical methods, and plasma

polymerization [6- 10].

Conducting polymers have many applications due to their distinctive properties, including controllable electronic properties, high theoretical capacitance, good wave absorption [11- 14], excellent electrochemical behavior, high redox activity [15- 17], ease of synthesis and fabrication, as well as their environmental stability, where they are used as anti-static coatings, membranes, sensors, energy storage and conversion devices, light-emitting diodes, display technologies, and corrosion protection of iron in acidic media [18- 20]. The stability of conducting polymers depends on the nature of the monomer, its concentration, and the synthesis temperature. To improve the conductive properties of the polymer films, it is necessary to control the different synthesis parameters.

Polyaniline and its derivatives occupy the most important place among conductive polymers due to their unique properties, including ease of preparation in aqueous media, good stability, ease of doping, and electrochromic effects [21- 25], and improved electronic properties achieved through either chemical or electrochemical polymerization. Chemical synthesis requires the use of strong oxidants, such as hydrogen peroxide or perchlorate, ammonium persulfate [26- 29]. In this study, poly (p-toluidine) (PPT) and starch-grafted poly (p-toluidine) copolymer (SGPPT) were prepared and analyzed by FTIR and UV-Vis Spectrophotometer, and studied kinetically and thermodynamically through the results of TG.

2. STUDY DESIGN

Toluidine and absolute ethanol were supplied by RDH, Fluka supplied starch, hydrochloric acid, ammonium persulfate, and sodium hydroxide.

Preparation of poly (p-toluidine). To prepare poly (p-toluidine), 3 g of (p-toluidine) monomer were dissolved in 200 mL of 1 M HCL aqueous solution (referred to as the first solution), which was then cooled to a temperature range of 273–277 K using an ice bath. Simultaneously, 0.54 M of ammonium persulfate was dissolved in 200 mL of 1 N HCl solution (referred to as the second solution). The second solution was added dropwise to the first solution under continuous stirring. Within minutes, the color of the reaction mixture changed to a darker brown hue. The resulting mixture was filtered through filter paper and washed with distilled water until the filtrate became neutral (acid-free). Subsequently, the obtained solid was dried in an electric oven for 12 hours, resulting in the polymer being ground into a fine powder [30].

Preparation of starch-poly (p-toluidine). To prepare starch-grafted poly(p-toluidine), 3 mL of (p-toluidine) were dissolved in 20 mL of 1 N HCl and mixed with 1 g of starch, previously dissolved in 20 mL of 1 N HCl. The mixture was transferred to a flask and maintained at 298 K under continuous stirring. After 30 minutes, 5 g of ammonium persulfate was added in a single portion, and stirring continued for an additional hour. A 5% aqueous solution of NaOH was used to neutralize and precipitate the copolymer [31]. Figure 1 shows the structure and reaction diagram of starch-doped poly(p-toluidine) copolymer.

ISSN: 0972-0626
Volume 29, Issue 07, July, 2025

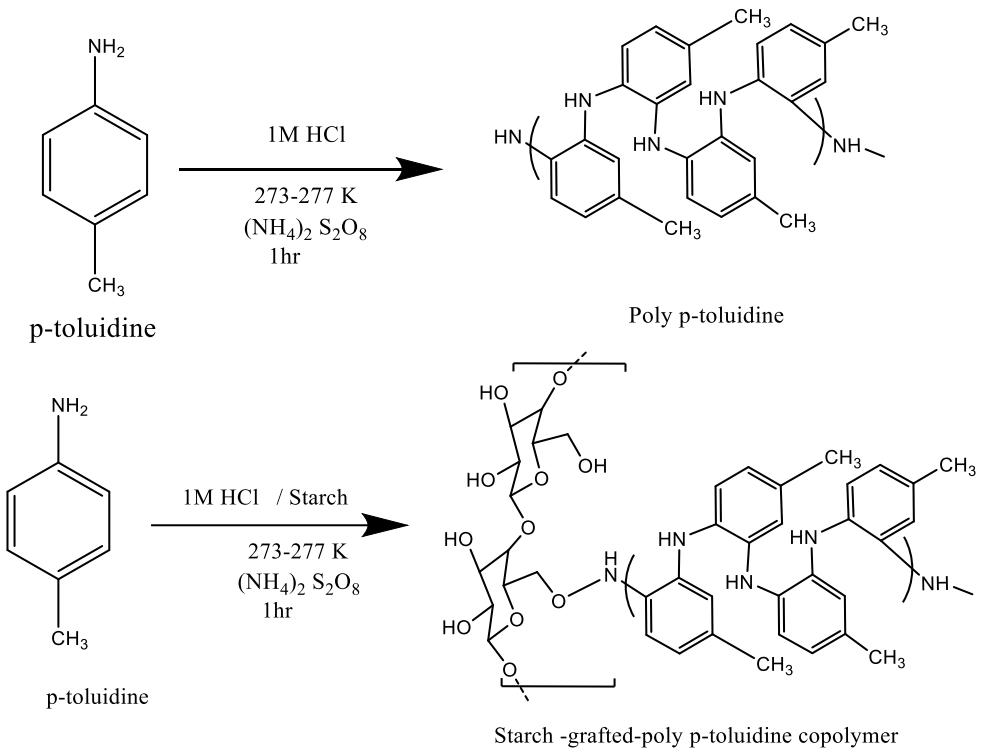

Figure No. 1 Scheme of structure and reaction of starch-grafted poly (p-toluidine) copolymer

3. Results and Discussion

FTIR of poly (p-toluidine) and grafting starch poly (p-toluidine) copolymer. The Fourier Transform Infrared Spectroscopy (FTIR) analysis was conducted on both poly (p-toluidine) and starch-grafted poly (p-toluidine) copolymer samples, as presented in Figures. 2 and 3 In the copolymer spectrum, distinctive peaks emerged, indicating structural modifications resulting from the grafting of starch onto the poly (p-toluidine) backbone. Notably, a prominent new peak appeared at 1575 cm^{-1}, corresponding to quinoid-benzenoid moieties in the copolymer structure. This peak indicates the incorporation of starch, suggesting a shift in the chemical environment surrounding the aromatic ring [32].

Additionally, the presence of the C=C stretching vibration of the aromatic ring was evidenced by a peak at 1514 cm^{-1}, further confirming the successful grafting of starch onto the poly (p-toluidine) matrix. This peak indicates the retention of the aromatic structure within the copolymer

Further analysis of the FTIR spectrum revealed a distinct peak at 2920 cm^{-1}, attributed to the C-H stretching vibrations of CH_3 groups within the poly (p-toluidine) component. This peak indicates the preservation of the poly (p-toluidine) backbone in the copolymer structure, albeit with modifications induced by the grafting process [33].

Moreover, a new peak at 1251 cm^{-1} was observed, corresponding to the C-N stretching vibrations of secondary amine groups originating from the (p-toluidine) component. This peak is indicative of the interaction between starch and poly (p-toluidine), further supporting the successful copolymerization process.

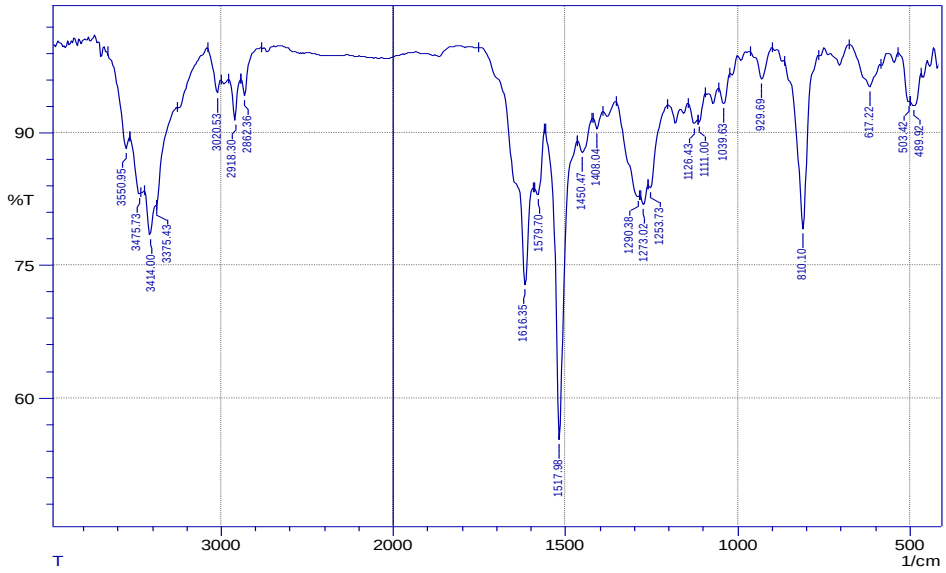

Figure No. 2 FTIR spectrum of PPT

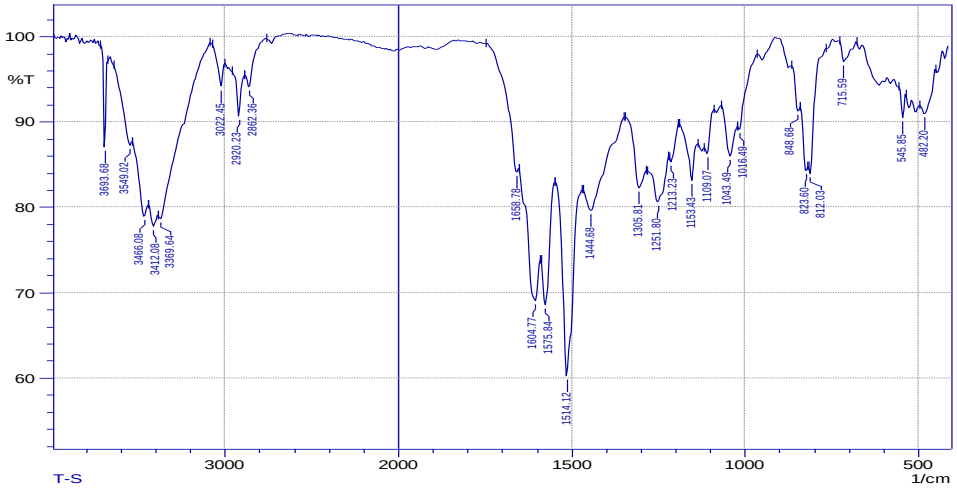

Figure No. 3 FTIR spectrum of SGPPT

UV-Vis Analysis. The optical properties of PPT and SGPPT were investigated using UV-Vis Spectrophotometer, as presented in the Figures. 4 and 5. Three slight bands were observed in the PPT spectrum at 250 and 279 nm. The bands are assigned as follows: the peak at 250 nm belongs to the π-π* transition of the benzenoid ring, the peak at 279 nm corresponds to the excitation coupling -π- polaron transition. [34] The overall appearance of SGPPT spectra was somewhat similar to that of PPT, with a clear increase in the absorption peak intensities due to the influence of starch on the polymer's electronic structure and molecular interactions, which can modify the energy levels thus confirming the formation of grafting [35]. The optical bandgap energy (E_g), was obtained using the Tauc's Plot as illustrated in Figures. 3 and 4 along with UV-visible spectra. Graphs of $(\alpha h\nu)^2$ versus photon energy ($h\nu$) were plotted and extrapolated. The obtained energy band gaps were found to be 3.52 eV and 2.37 eV for PPT and SGPPT, respectively. The grafting of starch with the structure of PPT increases absorption, which leads to a reduction in the energy band gap due to charge transfer transitions, and hence an increase in optical conductivity.

RJCE
ISSN:0972-0626
ISSN: 0972-0626
Volume 29, Issue 07, July, 2025

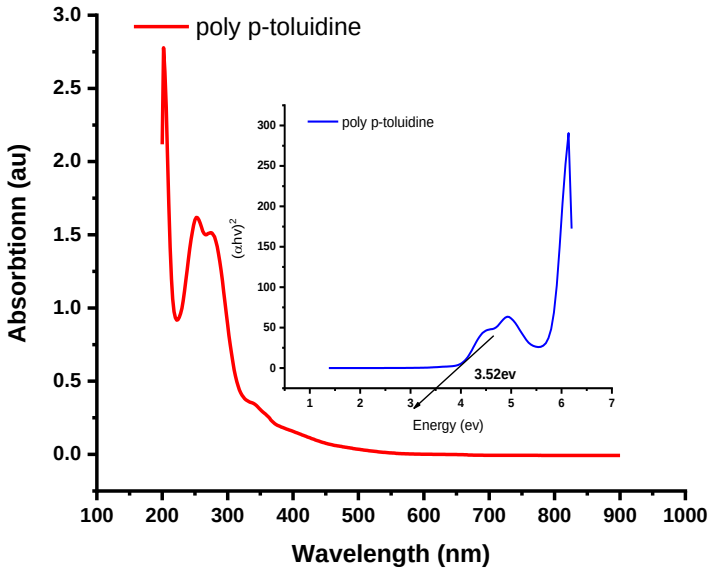

Figure No. 4 UV-Visible and Tauc's Plot of PPT

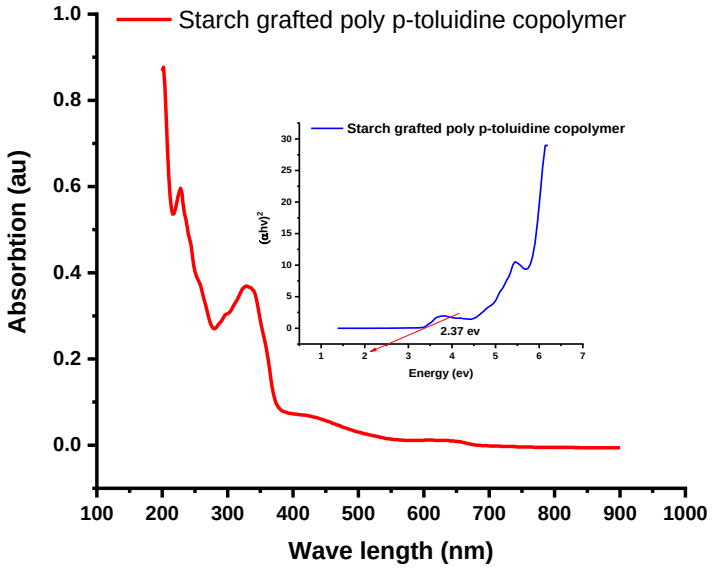

Figure No. 5 UV-Visible and Tauc's Plot of SGPPT

XRD analysis. The XRD patterns reveal a clear difference in the crystallinity between pure PPT and SGPPT, as presented in Figure .6. The SGPPT pattern exhibits distinct diffraction peaks with higher intensity [36, 37]. This indicates improved crystallinity due to the successful grafting of starch. This enhancement can be attributed to better molecular alignment and interaction between starch and polymer backbone.

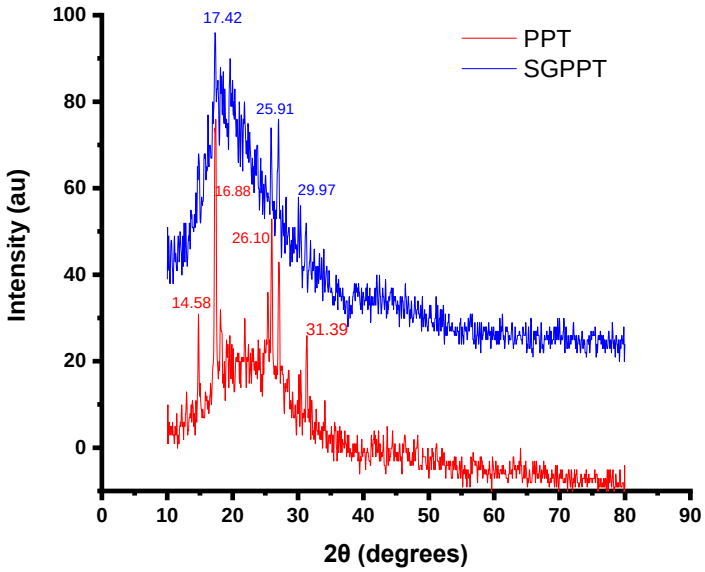

Figure No. 6 XRD pattern of PPT and SGPPT

FESEM analysis of SGPPT. In Fig. 7, the FESEM image of the SGPPT reveals a globular and moderately porous surface morphology, with particles in the nanoscale. The successful grafting of starch onto the poly (p-toluidine) backbone results a better-defined and interconnected structures, enhancing surface area and structural stability [38]. This morphology is favorable for applications such as electrochemical sensors and adsorptive materials.

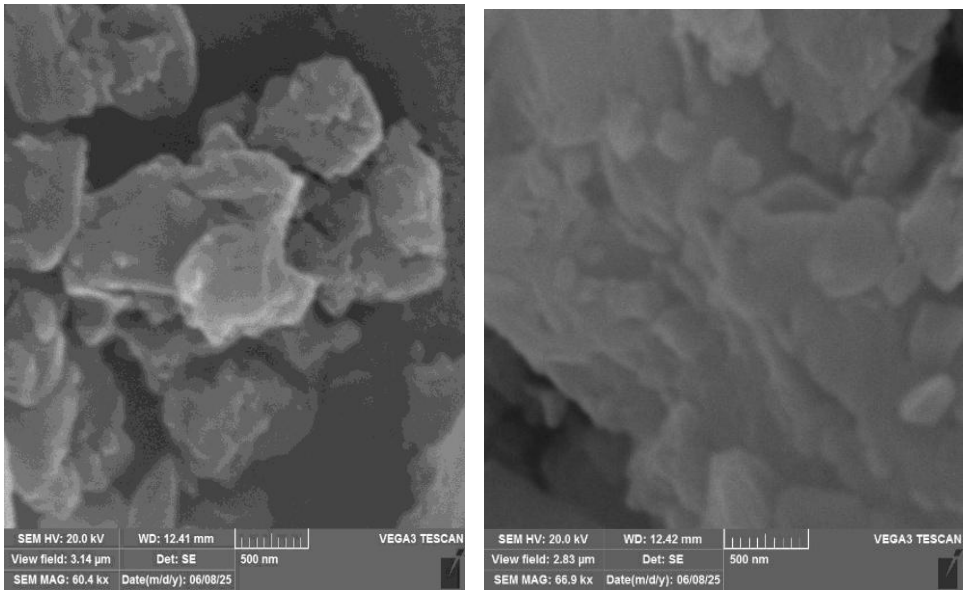

RJCE
ISSN:0972-0626
ISSN: 0972-0626
Volume 29, Issue 07, July, 2025

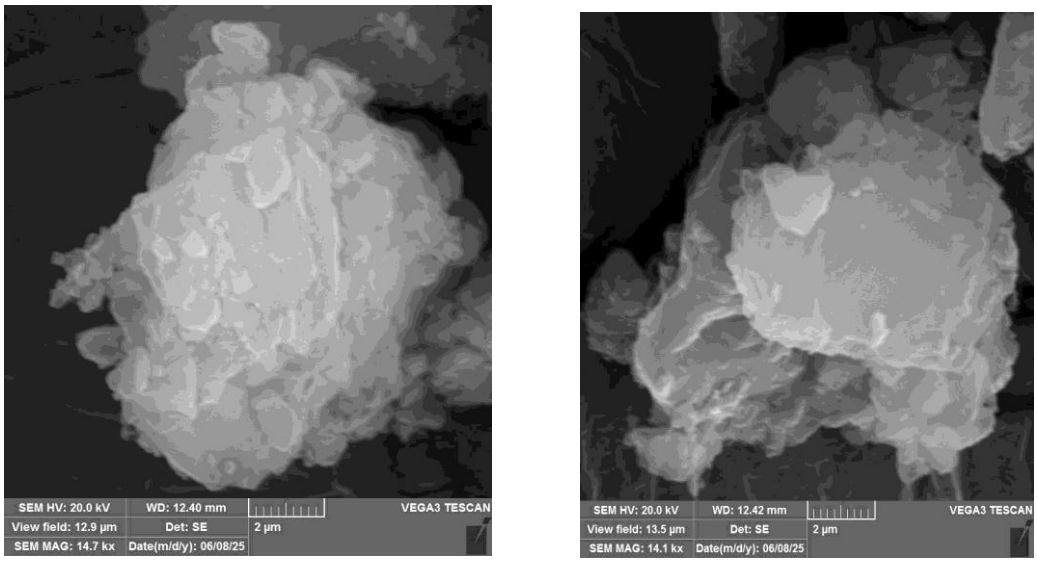

Figure No. 7 FESEM image of SGPPT

Thermodynamic and kinetic parameters from thermogravimetric analysis. From Thermogravimetric. First-order reaction considering. The transformation occurring in the polymer and copolymer is considered a first-order reaction. Thermodynamic parameters were determined using the first-order rate equation as given in Eq. (1) [36]

$$ln\,(1-x) = -kt \qquad (1)$$

$$x = \frac{wi-wt}{wi-wf} \qquad (2)$$

Where wi is the initial weight, wt is the weight of the sample at time t, and wf is the final weight. By plotting the values of ln(1−x) versus time, a straight line was obtained. The slopes were used to calculate the rate constant using the plotted graphs. The data followed a linear relationship according to Eq. (1); the slope of the line provided the value of the rate constant (k) (Fig. 8), and the half-life was determined using Eq. (3). [37]. The values of k and $t_{1/2}$ are listed in Table 2.

$$t_{1/2} = \frac{0.693}{k} \qquad (3)$$

Kinetic parameters were calculated using a modified form of the Coats–Redfern model, as described in Eq. (4).

$$ln[-ln(1-x)] = ln\frac{A\,RT^2}{\beta E_a} - \frac{E_a}{RT} \qquad (4)$$

Where A is the pre-exponential factor, β is the heating rate (20 °C/min), R is the universal gas constant (8.3143 $J\cdot mol^{-1}\cdot K^{-1}$), Ea is the activation energy, and T is the temperature in Kelvin. A plot of ln[(−ln(1−x))/T^2] versus 1/T (Fig. 10) was used to determine the activation energy. Additional thermodynamic parameters were obtained using the relevant equations shown in Table 1, confirming that the degradation processes of both the polymer and copolymer are non-spontaneous and endothermic in nature [38].

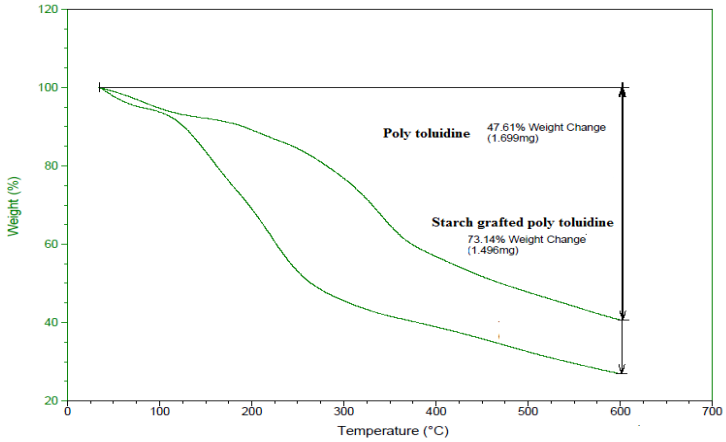

Figure No. 8 Thermogravimetric analysis of PPT and SGPPT

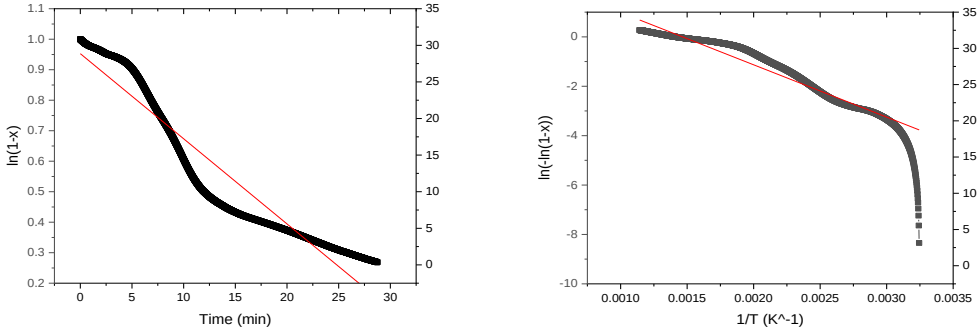

Figure No. 9 First order reaction of PPT

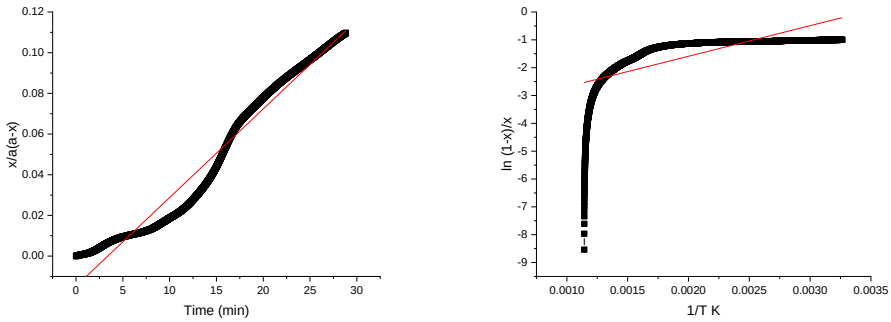

Figure No. 10 Second-order reaction of SGPPT

Table No. 1 Kinetic and thermodynamic parameters of (p-toluidine) polymer and starch-grafted poly (p-toluidine) copolymer

Polymer and copolymer	k	$t_{1/2}$ **min**	E_a $kJmol^{-1}$	ΔH $\mathrm{k}\,Jmol^{-1}K^{-1}$	ΔS $(\mathrm{J.mol^{-1}.K^{-1}})$	ΔG **(J.mol^{-1})** $(\times 10^4)$
Polytoluidine	8.762922 min^{-1}	0.079	17.60	10.33	-252.10	23.08

ISSN: 0972-0626
Volume 29, Issue 07, July, 2025

Starch grafting Poly P-toluidine	0.00436 $dm^3.mol^{-1}min^{-1}$	0.015	9.13	1.86	-918.86	80.57

Table 1 presents the kinetic and thermodynamic parameters for both (p-toluidine) polymer and starch-grafted poly (p-toluidine) copolymer. These parameters offer valuable insights into the reaction rates, energy requirements, and spontaneity of the polymerization process.

Starting with the kinetic aspects, the rate constant (k) and the half-life (t1/2) are key indicators of the reaction speed and the time required for half of the reactants to be consumed, respectively. For the (p-toluidine) polymer, the rate constant (k) is significantly higher at 8.76 ×10-3 min-1, indicating a relatively rapid reaction when compared to the starch-grafted poly (p-toluidine) copolymer, which has a much lower rate constant of 4.36×10^{-6} dm-3$mol^{-1}\cdot min^{-1}$.

This difference in reaction rates may be attributed to the variations in the chemical structure and composition of the two polymers.

Regarding the thermodynamic parameters, the activation energy (Ea) represents the energy barrier that must be overcome for the reaction to proceed. The (p-toluidine) polymer shows a higher activation energy of 79 kJ/mol compared to the starch-grafted poly (p-toluidine) copolymer with an Ea of 9.13 kJ/mol, implying that the latter requires less energy input for the reaction to occur, indicating a more facile process.

Moreover, the enthalpy (ΔH) and entropy (ΔS) changes provide insights into the heat absorbed or released and the randomness of the system during the reaction. The (p-toluidine) polymer exhibits a greater enthalpy change (ΔH = of 17.60 $kJ.mol^{-1}$) compared to (ΔH = 9.13 $kJ.mol^{-1}$) for the copolymer, indicating a greater heat absorption/release during the polymerization process. Similarly, the entropy change is higher for the p-toluidine) polymer (ΔS = 10.33 $J\cdot mol^{-1}\cdot K^{-1}$) than for the copolymer (ΔS = 1.86 $J\cdot mol^{-1}\cdot K^{-1}$), indicating a higher degree of randomness during the reaction.

The more negative ΔG value observed for the copolymer (-91.88×10^4 $J\cdot mol^{-1}$) compared to the (p-toluidine) polymer (-25.21×10^4 $J\cdot mol^{-1}$) indicates a greater thermodynamic favorability of the copolymerization process.

Conductive study. The present study aimed to evaluate the electrical conductivity of a polymer and its corresponding copolymer by fabricating thin films on aluminum substrates, using evaporated aluminum electrodes under low-pressure conditions. Conductivity measurements were performed at room temperature by varying the current with respect to the applied voltage, as illustrated in Figure 11.

The results showed that both the polymer and the copolymer exhibited ohmic behavior, as demonstrated by the linear current–voltage relationship. This characteristic is indicative of a consistent conductivity response across the range of applied voltages. This behavior indicates a stable and uniform conductivity response throughout the applied voltage range. Furthermore, the study demonstrated that the copolymer exhibits higher conductivity than the polymer [39].

The copolymer showed a conductivity of 0.358 Ω^{-1}, whereas the polymer recorded a slightly lower value of 0.294 Ω^{-1}. The observed difference in conductivity between the two materials can be attributed to several factors, including variations in molecular structure, chemical composition, and degree of polymerization. The

incorporation of co-monomers into the copolymer structure may have enhanced its electrical properties, resulting in improved conductivity compared to the homopolymer.

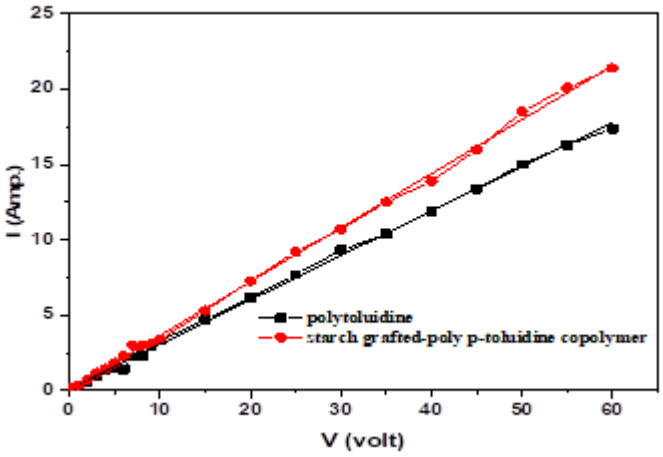

Figure No. 11 Relationship between current and voltage for PPT and SGPPT

Density Functional Theory (DFT) Study. The HOMO and LUMO energy values for starch, (p-toluidine), and poly (p-toluidine)-functionalized starch are presented in Tables 2 and 3. The computed energy gaps were analyzed to evaluate changes in the electronic band gap.

The electronic conductivity of a molecule is inversely related to its HOMO–LUMO energy gap. In this study, the HOMO–LUMO gap of the repeating unit of starch (α-D glucose) (7.78098545 eV) is significantly larger than those of glucose-grafted (p-toluidine) (0.46258694 eV) and glucose-grafted di-(p-toluidine) (0.254142008 eV), suggesting that functionalization enhances electronic conductivity.

The presence of toluidine within the starch–toluidine structure plays a key role in modifying the electronic properties by narrowing the energy gap. This functionalization increases the HOMO energy level while decreasing the LUMO level, thus facilitating easier electron transitions. In contrast, unmodified starch exhibits a larger energy gap, reflecting its lower conductivity. The addition of the toluidine monomer to the starch repeating unit results in a reduced energy gap, as shown in Table 3.

Furthermore, the theoretical results for the energy gap values are in good agreement with the experimental findings obtained from the Tauc plot, reinforcing the validity of the grafted copolymer's enhanced electronic behavior.

Table No. 2 Structures, optimized geometries, and HOMO–LUMO energy levels of PPT, SGPPT, and starch monomer [40]

n	Structure	Optimized Geometries	HOMO	LUMO
1	H_3C — NH_2 *p*-toluidine	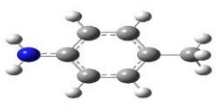	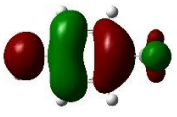	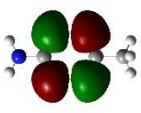

RJCE
ISSN:0972-0626
ISSN: 0972-0626
Volume 29, Issue 07, July, 2025

2	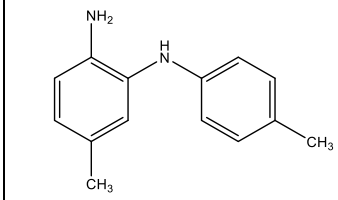	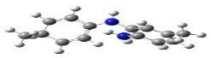	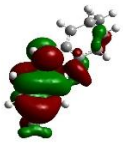	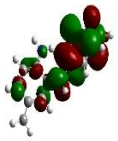
3	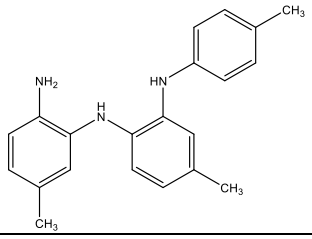			
4	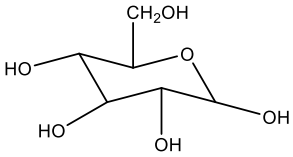	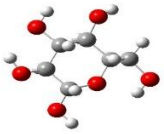	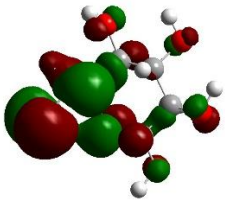	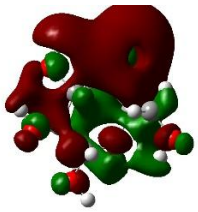
5	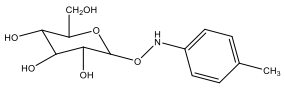	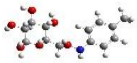	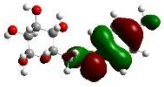	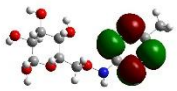
6	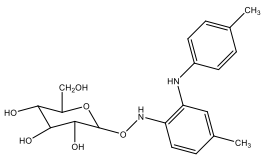	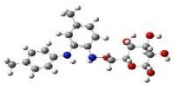		

Table No. 3 HOMO and LUMO Energy Values of Monomer, Polymer, and Copolymer Compounds [41]

No.	Compound	Total Energy (a.u.)	HOMO Energy (eV)	LUMO Energy (eV)	Energy Gap (ΔE, eV)
1	p-toluidine	-325.12696518	-4.88988858	0.51973774	5.40962632
2	α – D glucose	-683.3537169	-6.66451812	1.11646733	7.78098545
3	Di -p-toluidine	-649.60914402	-1.17959685	0.334287135	1.513883985

4	Tri-p-toluidine	-978.42649704	-0.02965999	0.17170141	0.34340282
5	α − D glucose − grafted p − toluiod	-1012.90715790	-0.01741504	0.4451719	0.46258694
6	α − D glucose − grafted di − p − toluiod	-1331.19450428	-0.004617168	0.24952487	0.254142008

4. Conclusion

In conclusion, the structures of these copolymers were confirmed by FTIR, XRD, UV-visible, and SEM techniques. SEM and XRD demonstrated that the copolymer's structure is more ordered than that of the pure polymer, exhibiting a granular shape at the nanoscale.

The kinetic and thermodynamic analyses provided a view into the polymerization processes of (p-toluidine) polymer and starch-grafted poly (p-toluidine) copolymer. Notably, (p-toluidine) polymerized at a significantly faster rate than the copolymer, while the copolymer generally exhibited lower activation energy and Gibbs free energy change values, indicating a more facile and spontaneous process. Additionally, conductivity studies demonstrated that both materials displayed ohmic behavior, but the copolymer exhibited higher conductivity compared to the polymer, likely due to factors such as molecular structure, chemical composition, and degree of polymerization. The incorporation of co-monomers in the copolymer structure likely contributed to its enhanced electrical properties. Additionally, DFT showed that the starch-functionalized poly (p-toluidine) has a smaller energy gap than the unmodified polymer, indicating better electrical conductivity, according to studies of the HOMO-LUMO energy gaps. This result illustrates the electronic effects of poly (p-toluidine), whereby molecular orbital modification lowers the energy gap and facilitates electron transport. Molecular design benefits greatly from these insights, especially for materials that need improved electrical characteristics.

5. Conflict of interest

No conflict of interest.

6. References

[1] Aprianti, N., Faizal, M., Said, S., & Fudholi. A. (2023) Gasification kinetic and thermodynamic parameters of fine coal using thermogravimetric analysis. *Energy*, 268, 126666. 10.1016/j.energy.2023.126666.

[2] Wang, Z., Wu, Z., Weng,L., Jiang,D., Huang, M., Jazzar, A., & He, X. (2023). A roadmap review of thermally conductive polymer composites: critical factors, progress, and prospects. *Advanced Functional Materials*, 33 (36), 2301549. 10.1002/adfm.202301549.

[3] Jebarshia, J., Preethi, T., Ashokan, S., Geetha ,N., & Senthil, K. (2024). Co-doped polyaniline composites for biological application: Morphological, functional, optical, and antibacterial activities. *Inorganic Chemistry Communications*, 161, 111971. 10.1016/j.inoche.2023.111971.

[4] Zhou, S., Jia,Q., Cui, L., Dai, Y., Tang, J., & Lu, J. (2023). Physical–chemical and sensory quality of oat milk produced using different cultivars. *Foods*, 12(6), 1165. 10.3390/foods12061165.

[5] Lade, J., Mohammed, K., Singh, D., Verma, P., Math, P., Saraswat, M., & Gupta, L. (2023). A critical review of fabrication routes and their effects on mechanical properties of AMMCs, *Materials, Today: Proceedings*. 10.1016/j.matpr.2023.03.041.

[6] Feng, J., Alves, J., de Clercq, D., & Schmidt, T. (2023). Photochemical upconversion. *Annual Review of Physical Chemistry*, 74(1), 145–168. https://doi.org/10.1146/annurev-physchem-092722-104952.

[7] Ahmed, S., Ahmed, A., Basha, D., Hussain, S., Uddin, I., & Gondal, M. (2023). Critical review on recent developments in conducting polymer nanocomposites for supercapacitors. *Synthetic Metals*, 295, 117326. 10.1016/j.synthmet.2023.117326.

[8] Wang,X., Yu,G., Zhang,J., Yu, M., Ramakrishna, S., & Long, Y. (2021). Conductive polymer ultrafine fibers via electrospinning: Preparation, physical properties and applications. *Progress in Materials Science*, 115, 100704. 10.1016/j.pmatsci.2020.100704.

[9] Bavatharani, C., Wabaidur, C., Alsheetan, M., & Ragupathy, M. (2021). Electrospinning technique for production of polyaniline nanocomposites/nanofibres for multi-functional applications: A review. *Synthetic Metals*, 27, 116609. 10.1016/j.synthmet.2020.116609.

[10] Jadoun, S., Fuentes, S., Urbano, F., & Yáñez, J. (2023). A review on adsorption of heavy metals from wastewater using conducting polymer-based materials. *Journal of Environmental Chemical Engineering* 11(1), 109226. 10.1016/j.jece.2022.109226.

[11] Liu, Y., Zhou, L., Wan, X., W. Li, W., & Liao, J. (2024). Synthesis and Characterization of a Temperature-Sensitive Microcapsule Gelling Agent for High-Temperature Acid Release. *ACS Omega*, 9(19), 20849–20858. 10.1021/acsomega.3c09586.

[12] Shen, P., Yin, P., Zou, M., Li, M., Li, B. (2023). Ultra-fast piezocatalysts enabled by interfacial interaction of reduced graphene oxide/MoS_2 heterostructures. *Advanced Materials*, 35(18), 2212172. 10.1002/adma.202212172.

[13] Wheeler, J., & Zozoulenko.I. (2024). Computational Microscopy of Spatial Dopant Distribution in Conjugated Polymer. *Advanced Electronic Materials*, 2400662, 1-7. 10.1002/aelm.202400662.

[14] Tadesse, M., Ahmmed, A., & Lübben, J. (2024). Review on conductive polymer composites for supercapacitor applications. *Journal of Composites Science*, 8(2), 53. 10.3390/jcs8020053.

[15] Chen, J., Zhu,Y., Huang, Zhang, J., & Guo, Z. (2021). Advances in responsively conductive polymer composites and sensing applications. *Polymer Reviews*, 61(1), 157–193. 10.1080/15583724.2020.1734818.

[16] Guo, X., X., Wang, F., Zhang, J., & Pan, L. (2022). Application of conductive polymer hydrogels in flexible electronics. *Journal of Polymer Science*, 60(18), 2635–2662. 10.1002/pol.20210933.

[17] Sharma, S., Sudhakara, P., & Ilyas, A. (2021). Recent trends and developments in conducting polymer nanocomposites for multifunctional applications. *Polymers*, 13(17), 2898. 10.3390/polym13172898.

[18] Liu, X., Zheng, W., Kumar, R., & Zhang, J. (2022). Conducting polymer-based nanostructures for

gas sensors. *Coordination Chemistry Reviews*, 462, 214517. 10.1016/j.ccr.2022.214517.

[19] Dan, L., & Elias, A. (2020). Flexible and stretchable temperature sensors fabricated using solution-processable conductive polymer composites. *Advanced Healthcare Materials*, 9(16), 2000380. 10.1002/adhm.202000380.

[20] Idumah. C.I. (2021). Novel trends in conductive polymeric nanocomposites, and bionanocomposites. *Synthetic Metals*, 273, 116674. 10.1016/j.synthmet.2020.116674.

[21] Tan, P., H. Wang, H., & Xiao, F. (2022). Solution-processable, soft, self-adhesive, and conductive polymer composites for soft electronics". Nature Communications. 13: 358. 10.1038/s41467-022-28027-y.

[22] M. Beygisangchin, S. Abdul Rashid, S. Shafie, A.R. Sadrolhosseini, and H.N. Lim. (2021). "Preparations, properties, and applications of polyaniline and polyaniline thin films—A review. *Polymers*, 13(12), 2003. 10.3390/polym13122003.

[23] Kazemi, F., Naghib, S., Zare, Y., & Rhee, K. (2021). Biosensing applications of polyaniline (PANI)-based nanocomposites: A review. *Polymer Reviews*, 61(3), 553–597. 10.1080/15583724.2020.1858871.

[24] Treto-Suárez, M., Diaz-Uribe, C., Vallejo,W., & Schott, E. (2023). New Polyaniline Derivative with Two Central Ester Groups: Synthesis, Characterization, and Theoretical Study. *ACS Omega*, 8(51), 48938–48945. 10.1021/acsomega.3c06471.

[25] Miraqyan,N., Durgaryan, R., & Durgaryan, N.. (2024). Synthesis and investigation of methyl and methoxy groups containing polyaniline derivatives in organic medium. *Polymer Bulletin*, 81(10), 8901–8915. 10.1007/s00289-023-05100-0.

[26] Andriianova, A., Salikhov, R., Latypova, L., & Mustafin, A. (2022). "The structural factors affecting the sensory properties of polyaniline derivatives". Sustainable Energy & Fuels. 6(14): 3435–3445. 10.1039/d2se00405d.

[27] El-Naggar, A., Heiba, Z., Kamal, A., Abd-Elkader, O., & Mohamed, M. (2023). Impact of ZnS/Mn on the structure, optical, and electric properties of PVC polymer. *Polymers*, 15(9), 2091. 10.3390/polym15092091.

[28] Wang, Q., Che, J., Wu,W., Hu, Z., Liu, X., & Zhang, J. (2023). Contributing factors of dielectric properties for polymer matrix composites. *Polymers*, 15(3), 590. 10.3390/polym15030590.

[29] Claro, F., de Lima, G., de Lima, T., Hansel, F., & Magalhães, W. (2023). Characterisation of laccase-mediated lignin polymerisation: implications for molecular weight, thermal stability, and electrical properties. *Biomass Conversion and Biorefinery*, 1–16. 10.1007/s13399-023-05040-9.

[30] Becke. A. (1997). Density-functional thermochemistry. V. Systematic optimization of exchange-correlation functionals. *The Journal of Chemical Physics*, 107(20), 8554–8560. 10.1063/1.475007.

[31] Frisch, A., Ireland, M., Rizzari, J., Lönnstedt, O., & Hobbs, A. (2016). Reassessing the trophic role of reef sharks as apex predators on coral reefs. *Coral Reefs*, 35, 459–472. 10.1007/s00338-016-1415-2.

[32] Lin, Q., Li, R., Zhang, F., Kai, K., Ong, Z., & Sato, H. (2023). Resilient conductive membrane synthesized by in-situ polymerisation for wearable non-invasive electronics on moving appendages of cyborg insect. *Npj Flexible Electronics*, 7(1), 42. 10.1038/s41528-023-00274-z.

[33] Li, Y., Zhou, M., Xia, Z., Gong, Q., Liu, X., Yang, Y., & Gao, Q. (2020). Facile preparation of polyaniline covalently grafted to isocyanate functionalized reduced graphene oxide nanocomposite for high performance flexible supercapacitors. Colloids and Surfaces A. *Physicochemical and Engineering Aspects*, 602, 125172. 10.1016/j.colsurfa.2020.125172.

[34] Alipour, A., Lakouraj, M., Hasantabar, V., Tashakkorian, H., & Mohseni.M. (2021). Evaluation of adsorption and biological activities of polyaniline-grafted-pectin as conductive nanogels. *Carbohydrate Polymer Technologies and Applications*, 2, 100151. 10.1016/j.carpta.2021.100151.

[35] Farrukh, M., Butt, K., Chong, K., & Chang, W. (2019). Photoluminescence emission behavior on the reduced band gap of Fe doping in CeO_2-SiO_2 nanocomposite and photophysical properties. *Journal of Saudi Chemical Society*, 23(5), 561–575. 10.1016/j.jscs.2018.10.002.

[36] Boutaleb, N., Chouli, F., Benyoucef, A., Zeggai, F., & Bachari, K. (2021). A comparative study on surfactant cetyltrimethylammoniumbromide modified clay-based poly(p-anisidine) nanocomposites: Synthesis, characterization, optical and electrochemical properties. *Polymer Composites*, 42(4), 1648–1658. 10.1002/pc.25941

[37] Raza, M., Abu-Jdayil, B., Al-Marzouqi, A., & Inayat, A. (2022). Kinetic and thermodynamic analyses of date palm surface fibers pyrolysis using Coats-Redfern method. *Renewable Energy*, 183, 67–77. 10.1016/j.renene.2021.10.065.

[38] Gautam, V., Srivastava, A., Singh, K., & Yadav, V. (2017). Preparation and characterization of polyaniline, multiwall carbon nanotubes, and starch bionanocomposite material for potential bioanalytical applications. *Polymer Composites*, 38(3), 496–506. 10.1002/pc.23608.

[39] Genies, E., Lapkowski, M., & Penneau, J. (1988). Cyclic voltammetry of polyaniline: interpretation of the middle peak. *Journal of Electroanalytical Chemistry and Interfacial Electrochemistry*, 249(1–2), 97–107. 10.1016/0022-0728(88)80351-6.

[40] Alsulami, Q., & Hussein, M. (2023). A Sequence Study on the Enhanced Charge Transfer of SWCNTs and CuO-Reinforced Poly(o-anisidine-co-o-toluidine) Nanocomposites. *Journal of Inorganic and Organometallic Polymers and Materials*, 33, 820–830. 10.1007/s10904-023-02539-6.

[41] Magalhães da Silva, S., Silva,M., & Oliveira, J. (2021). Non-isothermal cold crystallization kinetics of cork–polymer biocomposites based on polylactic acid for fused filament fabrication. *Journal of Thermal Analysis and Calorimetry*, 146(4), 1667–1678. 10.1007/s10965-022-03335-5.International License.